Supplementary Information

Multi-tier approach to investigate the trojan-horse effect of polystyrene nanoplastics towards triclosan

Authors:

Parenti[1], C.C., Magni[1], S., Ghilardi[1], A., Caorsi[1], G., Della Torre[1], C., Del Giacco[1], L., Binelli[1*], A.
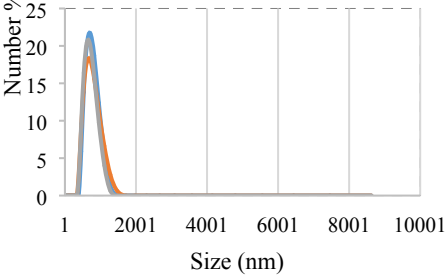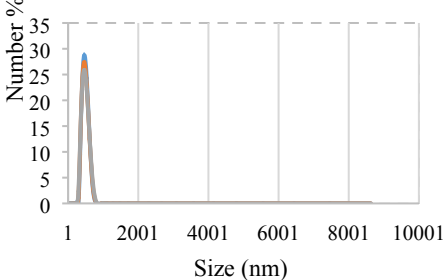
[1]Department of Biosciences, University of Milan, Via Celoria 26, 20133 Milan, Italy

*Corresponding author e-mail: andrea.binelli@unimi.it

2. EXPERIMENTAL

2.1 *PNPs characterization*

Table S1. Chemical parameters of PNPs measured by the Malvern Zetasizer Nano ZS instrument (Malvern instruments, UK) in the exposure medium. Data referred to a concentration of 1 mg/L. Size distribution is reported as average ± standard deviation of 3 measurements.

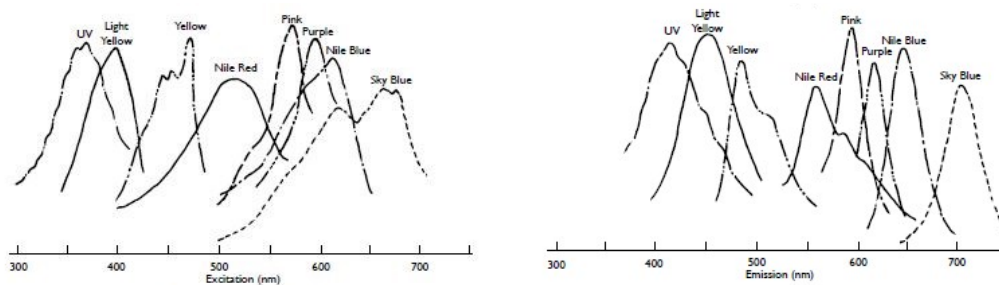| PNPs	Zeta-potential	Size distribution
No-fluo	-36.27 ± 0.67 mV	716.13 ± 23.14 nm
Fluo	-33.77 ± 0.38 mV	474.73 ± 2.34 nm

Fig. S1. Excitation and emission spectra of the fluorophore used in the fluorescent particles (Spherotech, Inc., Lake Forest, IL, USA).

2.2 *Biomarker*

To evaluate the levels of genotoxicity 7 larvae for each experimental group were pooled together and manually homogenized in PBS 0.01 M. First of all, cell viability was evaluated by the trypan blue dye exclusion method, mixing an aliquot of 10 µL of homogenates with 10 µL of 0.4% (w/v) trypan blue solution in PBS (three replicates per experimental group). Non-viable cells were stained deep blue. Later, the apoptotic and necrotic cell frequency (%) was assessed on 300 cells per slide (n = 9; three slides per pool), using a fluorescence microscope (Leitz DMR). An aliquot (10 µL) of homogenates was resuspended in LMA (Low Melting Agarose, 0.7% in PBS, pH 7.4), and distributed on slides pre-coated with a thin layer of NMA (Normal Melting Agorose, 1% PBS, pH 7.4). After fixation, slides were immersed in a lysis solution (NaCl 2.5 M, Na_2EDTA 100 mM, Tris-HCl 8 mM, pH 10) and maintained at 4°C in dark. Slides were then fixed in absolute ethanol. Before observations, cell nuclei were stained with DAPI. The frequency of micronuclei (MN ‰) was calculated on 400 cells per slide (n = 6; two slides per pool), using a fluorescence microscope (Leitz DMR). An aliquot (40 µL) of homogenates was distributed on slides and fixed for 15 min at real temperature (r.t). Slides were washed with glutaraldehyde solution (1% PBS) for 5 min, and PBS (0.01 M), and coloured for 5 min with bisbenzimide (Hoechst 33258, 1 µg/mL). In the end, samples were washed with a 1:1 glycerol:McIlvaine solution (1:1).

The effects on detoxification and antioxidant systems were evaluated on pools of 35 larvae (3 pools for each treatment) homogenized in potassium phosphate buffer pH 7.4 (100 mM), with the addition

of KCl (100 mM), EDTA (1 mM), protease inhibitors (1:100, v/v) and dithiothreitol (DTT; 1 mM). The homogenates were centrifuged at 15,000 g for 10 min at 4 °C and the recovered supernatants were used to measure the level of EROD, GST, SOD, CAT and GPx. EROD activity was evaluated by spectrofluorimetric analysis. Samples were added in a solution containing Tris (50 mM), BSA (5.32 g/mL in Tris), 7-ER (100 µM), and NADPH (3 mM). The reaction took place at 37°C in dark, in a thermostatic bath. After 20 min of incubation, samples were placed on ice and glycine (2 M) was added to terminate the reaction. A fast centrifugation at maximum speed was then applied to collect the supernatants and fluorescence was read at $\lambda_{ex/em}$=535/590 nm using the EnSight™ multimode plate reader. Results were normalized using a resorufine standard curve (0.001-1 µM) and a blank (Tris 50 mM). The GST activity was measured by adding reduced glutathione (1 mM) in phosphate buffer (100 mM, pH 7.4) and using CDNB (1 mM) as substrate. The difference in absorbance (ΔOD) was measured for 1 min at 340 nm using the spectrophotometer (Jenway, UK). SOD activity was determined by measuring the degree of inhibition of cytochrome c (10 mM) reduction by the superoxide anion generated by the xanthine oxidase (1.87 mU/mL)/hypoxanthine (50 mM) reaction at 550 nm. The activity was given as SOD units (1 SOD unit = 50% inhibition of the xanthine oxidase reaction). The CAT activity was determined by measuring the consumption of H_2O_2 (50 mM) in potassium phosphate buffer (100 mM, pH 7), measuring the ΔOD for 2 at 240 nm using the spectrophotometer (Jenway, UK). The GPx activity was assessed monitoring the consumption of NADPH at 340 nm using 0.2 mM H_2O_2 as substrate in 50 mM potassium phosphate buffer (pH 7) including glutathione (2 mM), sodium azide (NaN_3; 1 mM), glutathione reductase (2 U/mL), and NADPH (120 mM). The quantification of ROS was calculated using dichlorofluorescein diacetate (DCFH-DA), a pigment that emits fluorescence when oxidized. Samples were transferred into a 96 multi-well plate and incubated at r.t. for 5 min. Then, PBS and DFCH-DA (10 mg/mL) were added and the plate was incubated again for 30 min at 37 °C. The ROS concentration was measured by fluorescence at 485/530 nm (excitation/emission) using the Ensight™ multimode plate reader.

To assess the presence of a neurotoxic effect on exposed organisms, pools of 12 larvae were homogenized as described above. Samples (three replicates per experimental group) were transferred into a 96 multi-well plate adding phosphate buffer (100 mM, pH 7.4), 5,5'-dithiobis-2-nitrobenzoic acid (DTNB, 5 mM) and acetylthiocholine (ASCh, 1 mM). The activity level of AChE was assessed measuring fluorescence at 412 nm for 15 min using the EnSight™ multimode plate reader.

2.3 *Functional proteomics*

Pools of 20 larvae for each experimental group (3 pools for each treatment) were homogenized in a lysis buffer composed of (4-(2-hydroxyethyl)-1-piperazineethanesulfonic acid (HEPES) 20 mM pH 7.5, sucrose 320 mM, ethylenediaminetetraacetic acid (EDTA) 1 M pH 8.5, (ethylene glycol-bis(β-aminoethyl ether)-N,N,N',N'-tetraacetic acid (EGTA) 5 mM pH 8.1, sodium orthovandate (Na_3VO_4) 1 mM, β-glycerophosphate 10 mM, sodium fluoride (NaF) 10 mM, sodium pyrophosphate (NaPPi) 10 mM, phenylmethylsulfonyl fluoride (PMSF) 1 mM in ethanol, dithiothreitol (DTT) 5 mM e protease inhibitors (Roche) in Milli Q® water[1]. Homogenates were centrifuged at 15,000 g for 10 min at 4 °C and proteins were quantified in the supernatant using the Bradford method[2]. Then, 200 μg of proteins for each group were precipitated in a procedure using methanol/chloroform/Milli Q® water (4:1:3 v/v). The pellets were suspended again in a solution of urea 8 M in Tris-HCl 50 mM, sodium chloride (NaCl) 30 mM pH 8.5 and protease inhibitors (Roche). Samples were centrifuged at 14,000 g for 30 min at 4 °C and proteins were re-quantified. Then, 10 μg of proteins were incubated in DTT 50 mM in ammonium bicarbonate (AMBIC) 50 mM for 30 min at 52 °C under stirring to reduce the disulphide bonds. Later, iodoacetamide (IANH2) 100 mM in AMBIC 50 mM was added and samples were incubated for 20 min at room temperature (r.t.) under stirring to alkylate the sulfhydryl groups. Proteins were then digested adding trypsin (Trypsin Sequencing Grade, Roche, Italy) in AMBIC 50 mM and samples were incubated over-night at 37 °C under stirring. Peptides were then purified by reverse phase chromatography, using Zip Tips (μ-C18; Millipore, Milan, Italy; Magni et al., 2019). In particular, peptides were purified and analysed at UNITECH OMICs (University of Milan, Italy)

by the Dionex Ultimate 3000 nano-LC (Sunnyvale CA, USA) in connection with the Orbitrap Fusion™ Tribrid™ Mass Spectrometer (Thermo Scientific, Bremen, Germany). Proteins were identified using the Proteome Discoverer software 2.2 (Thermo Scientific) against the research database Uniprot-zebrafish.fasta and setting trypsin as digestive enzyme.

We measured the differences in abundance ratio (AR) between treatments and control for the total of identified proteins (minimum of two identified peptides). Two significance thresholds were applied on the entire dataset to guarantee the goodness of data and the biological meaning, based respectively on the p value ($p < 0.05$) and a minimum of 2-fold change difference in comparison with controls.

3. RESULTS

3.1 *Effects at individual level*
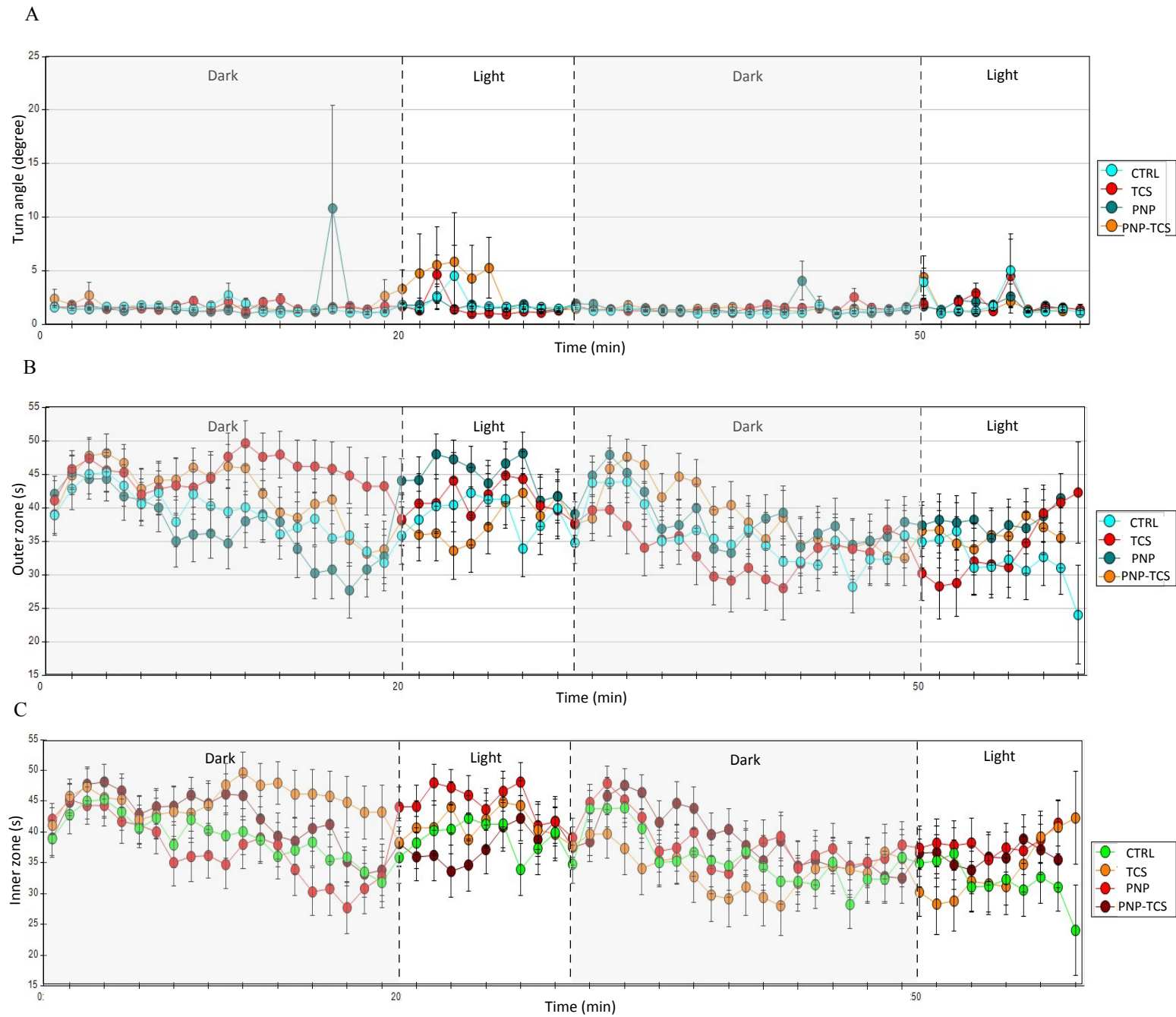
Fig. S2. Swimming activity measured in zebrafish larvae exposed to PNP (200 µg/L), TCS (0.6 µg/L) and PNP-TCS, compared to control. (A) Turn angle per minute (mean±S.E.); (B) Time spent in the outer zone per minute (mean±S.E.); (C) Time spent in the inner zone per minute (mean±S.E.).
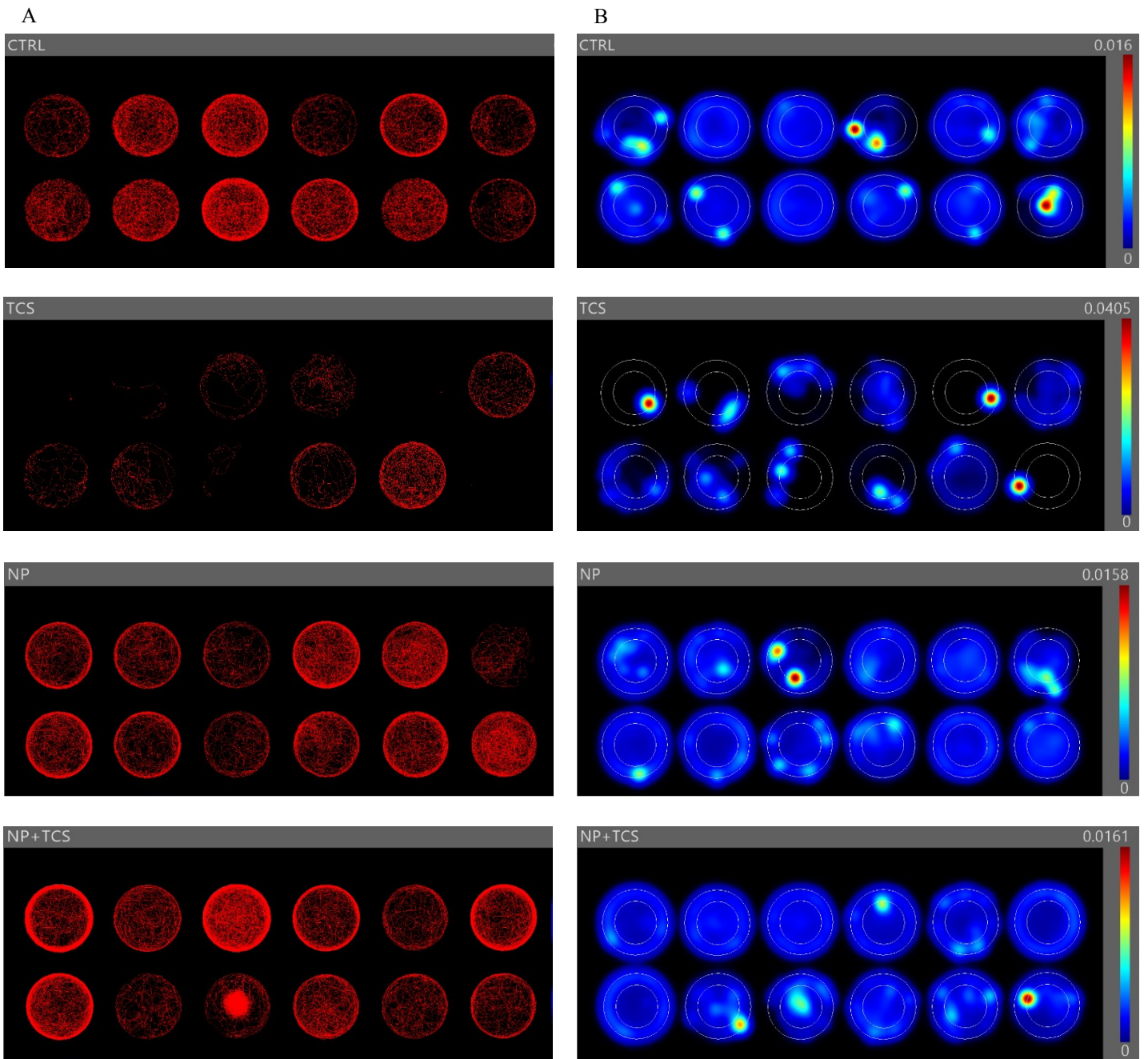
Fig. S3. Graphical representations of larval swimming activity, for each experimental group (data from one exposure). (A) Tracks; (B) Heatmaps.

4. DISCUSSION

4.1 *Effects on proteome*

4.1.1 *Proteins involved in genetic processes*

All the 5 proteins involved in genetic processes modified by the PNP-TCS complex (ELAV-like protein, *Elavl4*; TAR DNA-binding protein, *Tardbpl*; UDP-N-acetylhexosamine pyrophosphorylase-like protein 1, *Uap1/1*; heterogeneous nuclear ribonucleoprotein C1/C2, *Hnrnpc*; importin subunit α, *Kpna4*) were in common with TCS and were co-regulated in the same way (Fig. 6A). Three of them (*Elavl4*, *Tardbpl*, *Hnrnpc*) revealed also the same molecular function based on the RNA binding and belong to the RNA recognition motif (RRM) family that is known to selectively bind single-stranded RNAs[3]. RRM is one of the most abundant protein domains in eukaryotes and it is able to bind a multitude of RNA sequences and proteins. Eukaryotic RRM proteins are present in all post-transcriptional events, such as pre-mRNA processing, splicing and alternative splicing, mRNA stability and export, RNA editing, translation regulation and degradation[4].

Specifically, *Elavl4*, also known as *HuD*, is implicated in the early stage (from 14 hpf) of differentiation and specification of individual neurons in the development of zebrafish nervous system[5]. Akten et al.[6] pointed out a new interaction between *HuD* and the survival motor neuron (SMN) protein in spinal motor axons that selectively bind the cpg15-mRNA, whose transport and translation deficit are associated with some neurologic disorders, such as the fragile X syndrome and tuberous sclerosis[7,8]. The observed down-regulation of *Elavl4* can suggest a decreased capability to form the SMN-*HuD* complex with the consequence of negative effects on the development of motor axons and neuromuscular junctions due to TCS both alone and bound to PNPs.

The role played by *Tardbpl* in zebrafish is more complicated because it represents the homologue of *Tardbp*, whose orthologue *TARDBP* is implicated in the amyotrophic lateral sclerosis (ALS) in humans[9]. Very interestingly, Kabashi et al.[10] pointed out that the knockdown of *Tardbp* in zebrafish generated shorter and disorganized motor neuron axons and reduced coiling ability, while the knockdown of the homologue *Tardbpl* did not generate any defects. Hewamadduma et al.[11] showed

that *tardbp* mutation leads to the generation of a novel *tardbpl* splice form able of making a full-length *Tardbp* protein (*Tardbpl-FL*), which compensates for the loss of *Tardbp*. Since *Tardbpl* seems to be the product of alternative splicing able to block some neurogenerative disorders, its downregulation observed after the exposures to TCS and PNP-TCS complex could represent another signal of possible negative effects on the nervous system development in zebrafish, as also suggested by the modulation of *Elavl4*.

The role played by *Hnrnpc* is still little known. The KEEG PATHWAY Database highlighted that this protein is involved in the RNA binding and specifically belongs to the spliceosome protein complex that assemble on the mRNA precursor and help fold it for the subsequently transesterification.

The other two proteins co-modulated by TCS and PNP-TCS involved in genetic processes were the UDP-N-acetylhexosamine pyrophosphorylase-like protein 1 (*Uap1/l*) and importin subunit α (*Kpna4*) which are related to the nuclear import signal receptor activity and nuclear localization sequence binding, respectively.

4.1.2 *Catalytic proteins*

All the three contaminants impacted also on some proteins involved in catalytic activity, of which only the glutamine synthetase (*Gs*) are in common among the three treatments (Fig. 6A). *Gs* catalyzes several metabolic reactions, being a fundamental enzyme to maintain in fish the amino acid balance, neurotransmitter regulation and the biosynthesis of nucleotides and urea[12-14]. The simultaneous downregulation observed for *Gs* is particularly interesting in the light of its specific function related to the ammonia catalysis by the condensation of glutamate and ammonia into glutamine to counteract the ammonia increase in the body[15]. This means a possible disfunction in the ammonia elimination for zebrafish larvae mainly due to TCS exposure that downregulated also the above-mentioned *Atp6v1a* also related to this crucial function. Indeed, *Gs* activity is generally high in the brain of fish[16] to protect this organ from the harmful effect of ammonia, even if it is present also in other organs,

such as liver, muscle, kidney, stomach and intestine[15]. The need of the well-functioning of this enzyme is proven by the accumulation of ammonia in the extra- and intracellular compartments of fish exposed to high levels of this chemical in the aquatic ecosystems that can drive to convulsion, coma and death[17]. For instance, Wright et al.[18] found a significant (p<0.05) increase of Gs activity in brain and liver of rainbow trout ($O.$ $mykiss$) exposed to high level of NH_4Cl for 48 h, while Dhanasiri et al.[15] demonstrated a rise of Gs enzyme activity in response to increased ammonia levels in zebrafish exposed to high level of ammonia in water during 72 h simulated transport. This impact on the ammonia elimination should be in-depth investigated because it is the first time that this very dangerous effect for fish larvae linked to both PNPs and TCS exposures has been identified.

The F-box protein 2 ($Fbox2$) was the other in common regulated protein belong to catalytic group, with a difference to the other changed ones because it was upregulated by TCS but downregulated by PNP-TCS complex (Fig. 6A). $Fbox2$ is a neuron-enriched ubiquitin ligase substrate adaptor subunit that binds specifically glycoproteins containing high-mannose oligosaccharides, contributing to ubiquitination of N-glycosylated proteins through the endoplasmic reticulum-associated degradation (ERAD)[19]. This function is particularly important for the amyloid precursor protein (APP), a membrane glycoprotein whose degradation by-product showed the accumulation in Alzheimer disease[20]. However, APP is not only involved in the most common neurodegenerative disorder, but it has several roles in neuronal function and development, such as synapse formation, neurite outgrowth and neuronal survival[21,22]. Very intriguing, Atkin et al.[23] demonstrated as APP is not only a substrate for $Fbox2$, but also that it decreased in non-neuronal cells in the presence of $Fbox2$, while increased in hippocampal neurons and brain tissues in $Fbox2$ knock-out mice. This opens interesting questions about the possible role played by TCS to affect this protein with the fundamental function of APP regulation and its possible implication in the Alzheimer disease. We have not a clear explanation for the opposite regulation of $Fbox2$ due to TCS alone and PNP-TCS complex; one of the possible hypotheses could be due to the translocation of TCS in different neuron compartments mediated by the PNPs and the consequent different effect on this protein.

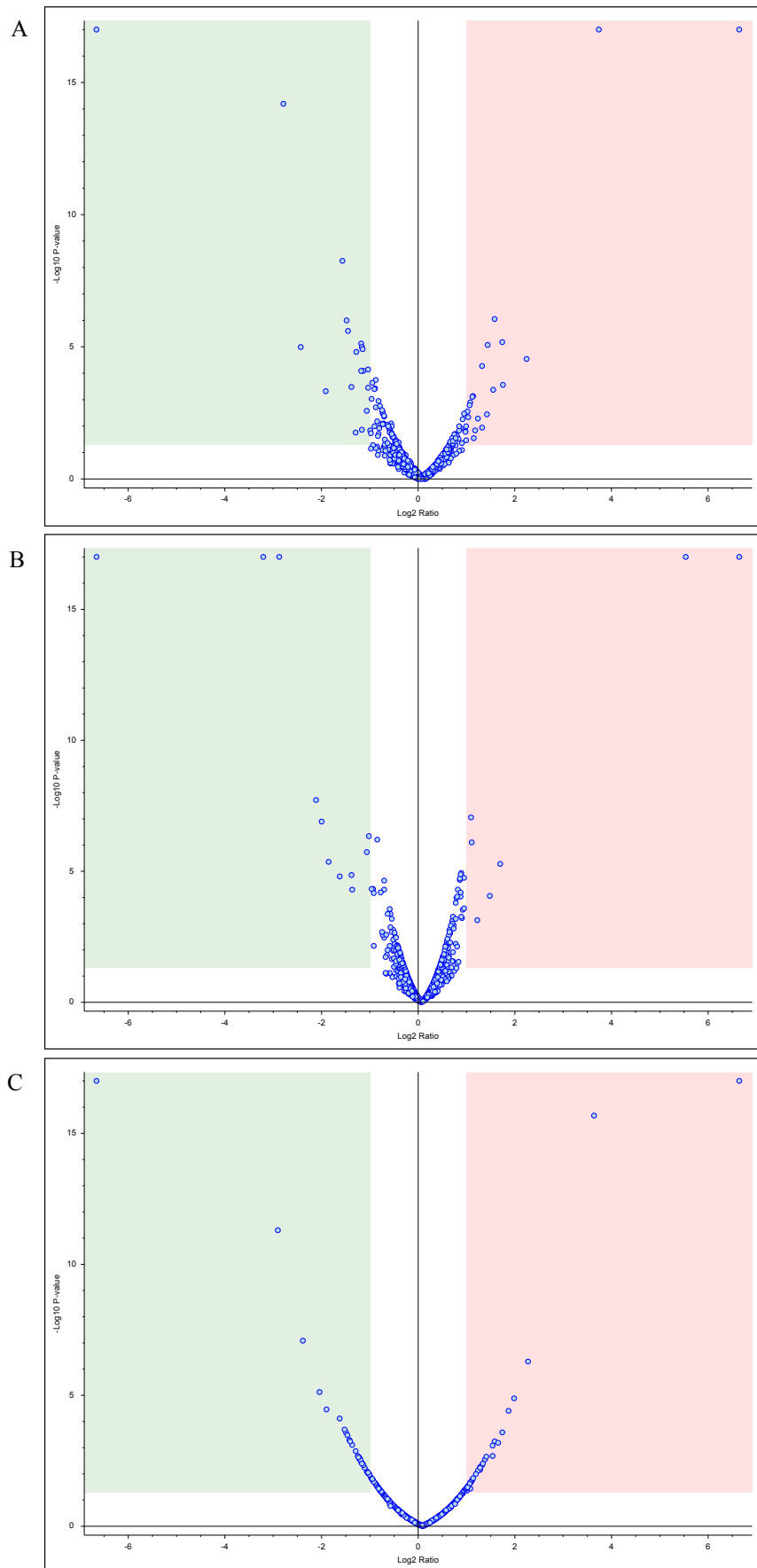**Fig. S4.** Volcano plots illustrating significantly differentially modulated proteins in zebrafish larvae exposed to (A) PNP (200 µg/L), (B) TCS (0.6 µg/L) and (C) PNP-TCS. The green and red squares denote ±2-fold change and p<0.05, which are the significance thresholds (prior to logarithmic transformation).

Table S2. Description of modulated proteins in zebrafish larvae exposed to PNP (200 µg/L), TCS (0.6 µg/L) and PNP-TCS, compared to control. MW = Molecular Weight, pI = isoelectric point, AR = Abundance Ratio, a = not significant value (p>0.05).

Main Function	UniProt Accession	Description	Peptides	Unique Peptides	MW (kDa)	pI	AR: PNP/CTRL	AR: TCS/CTRL	AR: PNP-TCS/CTRL
Cytoskeleton structure									
	C5IG37	beta-actin	19	1	24.8	5.31	0.603[a]	0.641[a]	0.409
	A9JRS6	keratin 4	47	2	54.0	5.39	0.443	0.938[a]	0.489[a]
	Q7ZVD3	lim-domain binding factor 3a	5	2	31.6	9.04	0.557[a]	0.109	NOT FOUND
	F1QVX3	myosin, heavy chain b	64	3	222.5	5.90	13.419	0.780[a]	12.551
	B3DJM6	myosin, heavy polypeptide 1, skeletal muscle	165	7	222.0	5.67	3.010	0.943[a]	3.959
	B8A569	myosin, heavy polypeptide 1.3, skeletal muscle	161	6	222.1	5.69	2.031[a]	0.716[a]	3.673
	Q6IQX1	myosin, heavy polypeptide 2, fast muscle-specific	151	11	221.7	5.69	2.201	0.914[a]	3.007
	Q6DHF0	myozenin 1b	5	1	28.8	5.60	0.507[a]	0.953[a]	0.357
	A0A286YBE9	plectin a	4	2	543.8	7.03	100.000	1.226[a]	100.000
	F1Q4X3	si:dkey-222n6.2	4	2	44.1	5.41	4.782	100.000	100.000
	A0MQ61	slow myosin heavy chain 1	43	14	222.8	5.66	2.728	1.038[a]	4.834
	B8A6B8	thymosin beta	2	2	5.2	8.47	0.385	1.046[a]	0.772[a]
	A5X6X6	titin b	83	1	3198.2	6.33	2.229[a]	1.686[a]	3.152
	Q9PUB6	type i cytokeratin	32	1	46.7	5.49	1.944[a]	46.817	2.033[a]
Immune system									
	F1Q7P7	pdgfa associated protein 1b	3	1	19.9	9.19	0.187	0.231	0.193
Genetic processes									
	Q7ZUQ9	cirbp protein	10	1	19.2	9.31	0.455	0.618[a]	0.546[a]
	F1R6L3	cold-inducible rna-binding protein b	11	2	23.6	8.84	0.489	0.764[a]	0.450[a]
	Q4V914	core histone macro-h2a	10	10	39.8	9.83	2.129	0.875[a]	2.191[a]
	F1R133	elav-like protein	10	1	45.0	9.28	0.145	0.138	0.134
	Q6NYV3	h1 histone family, member 0	5	4	21.2	10.86	2.096	1.071[a]	1.796
	A0A140LGU1	heterochromatin protein 1,-binding protein 3	19	19	66.8	9.67	2.191	0.941[a]	1.837[a]
	X1WDH8	histone h2b	11	1	13.5	10.21	3.346	NOT FOUND	NOT FOUND
	Q6PUQ6	importin subunit α	2	1	59.0	5.24	0.268	0.252	0.245

	Accession	Protein name							
Energy source/production									
	A0A0R4I9N0	purine-rich element-binding protein ab	3	2	31.3	7.49	100.000	0.823[a]	0.794[a]
	A0A2R8PYV5	tar dna-binding protein,-like	6	1	34.5	6.61	NOT FOUND	0.010	0.010
	A0A2R8RZT8	udp-n-acetylhexosamine pyrophosphorylase-like protein 1	2	1	56.3	5.94	0.878[a]	100.000	2.917
	A0A0R4IKH3	zgc: 55733 (heterogeneous nuclear ribonucleoprotein c1/c2)	2	1	32.5	5.66	0.408[a]	0.327	0.271
Catalytic activity									
	E7FCD8	atpase h+-transporting v1 subunit ab	15	1	68.3	5.58	1.553[a]	0.391	0.573[a]
	A0A1L1QZG0	chaperonin containing tcp1, subunit 2 (beta)	6	1	11.2	5.01	2.688[a]	2.353	2.675[a]
	Q6P969	elongation factor 1-alpha	9	2	50.3	9.07	2.947	3.267	1.237[a]
	A0A2R8QMC2	fructose-bisphosphate aldolase	2	1	40.5	7.02	100.000	100.000	0.870[a]
	A0A0R4ISN6	glutaryl-coa dehydrogenase b	3	2	17.0	8.19	0.692[a]	0.483	0.571[a]
	Q6IQP1	glycogenin 1b	2	1	36.0	5.49	0.010	0.010	0.010
	Q6TNR9	phosphoglycerate mutase	8	1	28.8	7.18	0.675[a]	0.949[a]	0.326
	B2GTJ4	rab5a protein	4	1	23.4	8.13	0.010	NOT FOUND	0.010
	B2GRK9	tkt protein	21	1	68.0	7.20	100.000	0.800[a]	1.421[a]
Transport									
	E9QDI1	apolipoprotein c-i	4	4	9.9	5.41	0.448	0.862[a]	0.439[a]
	A0A286YAE3	apolipoprotein c-ii	3	3	12.7	5.90	0.368	0.776[a]	0.445[a]
	Q6TEP3	glutamine synthetase	2	1	42.0	6.84	0.010	0.010	0.010
	Q3YA99	integrin beta	2	1	86.5	5.66	1.093[a]	0.886[a]	0.376
	A0A2R8QDD8	protein phosphatase, mg2+/mn2+-dependent, 1aa	3	1	43.0	5.30	NOT FOUND	NOT FOUND	0.010
	Q6PC06	s-adenosylhomocysteine hydrolase-like 2	6	1	65.0	7.61	0.010	NOT FOUND	NOT FOUND
	F8W4J1	serine protease 59, tandem duplicate 2	6	6	28.0	5.03	1.082[a]	2.137	1.112[a]
	B0BLX4	zgc: 175088 (f-box protein 2)	5	1	20.0	4.44	0.511[a]	100.000	0.423
	B3DIZ3	zgc:171967	4	1	104.1	5.40	0.620[a]	0.386	0.449[a]
Calcium metabolism									
	A0A2R8QJH4	calcium-transporting atpase	4	2	110.7	5.45	NOT FOUND	0.010	0.010[a]
	Q5BLF6	hemoglobin beta embryonic-3	6	1	16.6	8.44	3.403	100.000	1.339[a]
	B3DGI9	translocase of inner mitochondrial membrane 8 homolog b	2	2	10.7	5.80	0.360	0.733[a]	0.350

	Q804W0	parvalbumin 1	11	8	11.4	4.64	0.492	0.888[a]	0.531[a]
	Q5U3P2	parvalbumin 8	6	5	11.9	4.64	0.452	0.824[a]	0.654[a]
	Q6XG62	protein s100	9	4	10.4	5.21	0.442	0.841[a]	0.430[a]
Developmental processes									
	F8W2I6	galectin	5	1	15.3	7.94	0.885[a]	2.157	0.823[a]
Structural activity									
	A0A0R4IP59	collagen, type xiv, alpha 1b	5	5	84.5	5.35	1.436[a]	0.932[a]	2.918
	A0A2R8Q1I4	crystallin, gamma m2d2	9	1	21.4	7.81	0.986[a]	1.227[a]	3.350
Other									
	A7MBR3	pdz domain-containing 1	5	5	60.5	5.99	0.612[a]	1.121[a]	0.389
	X1WDJ4	si:dkey-248g15.3	2	2	7.8	8.50	0.414	0.497	0.363
	A0A0R4ITV0	si:dkey-46i9.1	2	2	7.3	5.45	0.338	0.675[a]	0.380

5. REFERENCES

1. A. Binelli, L. Del Giacco, N. Santo, L. Bini, S. Magni, M. Parolini, L. Madaschi, A. Ghilardi, D. Maggioni, M. Ascagni, A. Armini, L. Prosperi, L. Landi, C. La Porta and C. Della Torre, Carbon nanopowder acts as a Trojan-horse for benzo(α)pyrene in *Danio rerio* embryos, *Nanotoxicol.*, 2017, **11(3)**, 371-381.

2. M. M. Bradford, A rapid and sensitive method for the quantification of microgram quantities of protein using the principle of protein-dye binding, *Anal. Biochem.*, 1976, **72**, 248-254.

3. C. Maris, C. Dominguez, and F. H. T. Allain, The RNA recognition motif, a plastic RNA-binding platform to regulate post-transcriptional gene expression, *FEBS J.*, 2005, **272(9)**, 2118-2131.

4. E. Birney, S. Kumar and A. R. Krainer, Analysis of the RNA-recognition motif and RS and RGG domains: Conservation in metazoan pre-mRNA splicing factors, *Nucleic Acids Res.*, 1993, **21**, 5803-5816.

5. H. C. Park, S. K. Hong, H. S. Kim, S. H. Kim, E. J. Yoon, C. H. Kim, N. Miki and T. L. Huh, Structural comparison of zebrafish Elav/Hu and their differential expressions during neurogenesis, *Neurosci. Lett.*, **279**, 81-84.

6. B. Akten, M. J. Kye, L. T. Hao, M. H. Wertz, S. Singh, D. Nie, J. Huang, T. T. Merianda, J. L. Twiss, C. E. Beattie, J. A. J. Steen and M. Sahin, Interaction of survival of motor neuron (SMN) and HuD proteins with mRNA cpg15 rescues motor neuron axonal deficits, *PNAS*, 2011, **108**, 10337-10342.

7. H. Wang, Dynamic association of the fragile X mental retardation protein as a messenger ribonucleoprotein between microtubules and polyribosomes, *Mol. Biol. Cell.*, 2008, **19**, 105-114.

8. D. Nie, A. Di Nardo, J. M. Han, H. Baharanyi, I. Kramvis, T. Huynh, S. Dabora, S. Codeluppi, P. P. Pandolfi, E. B. Pasquale and M. Sahin, Tsc2-Rheb signaling regulates EphA-mediated axon guidance, *Nat. Neurosci.*, 2010, **13(2)**, 163-172.

9. M. Neumann, D. M. Sampathu, L. K. Kwong, A. C. Truax, M. C. Micsenyi, T. T. Chou, J. Bruce, T. Schuck, M. Grossman and C. M. Clark, L. F. McCluskey, B. L. Miller, E. Masliah, I. R. Mackenzie, H. Feldman, W. Feiden, H. A. Kretzschmar, J. Q. Trojanowski and V. M-Y. Lee, Ubiquitinated TDP-43 in frontotemporal lobar degeneration and amyotrophic lateral sclerosis, 2006, *Science*, **314**, 130-133.

10. E. Kabashi, L. Lin, M. L. Tradewell, P. A. Dion, V. Bercier, P. Bourgouin, D. Rochefort, S. Bel Hadj, H. D. Durham, C. Vande Velde, G. A. Rouleau and P. Drapeau, Gain and loss of function of ALS-related mutations of TARDBP (TDP-43) cause motor deficits in vivo, *Hum. Mol. Genet.*, 2010, **19(4)**, 671-683.

11. C. A. A. Hewamadduma, A. J. Grierson, T. P. Ma, L. Pan, C. B. Moens, T. Ramesh and P. J. Shaw, Tardbpl splicing rescues motor neuron and axonal development in a mutant tardbp zebrafish, *Hum. Mol. Genet.*, 2013, **22**, 2376-2386.

12. P. J. Walsh and T. P. Mommsen, in *Evolutionary considerations of nitrogen metabolism and excretion*, ed. P. Wright and P. Anderson, Academic Press, San Diego, 2001, Nitrogen excretion, 1-30.

13. P. Anderson, in *Urea and glutamine synthesis: environmental influences on nitrogen excretion*, ed. P. Wright and P. Anderson, Academic Press, San Diego, 2001, Nitrogen excretion, 239-277.

14. I. Suárez, G. Bodega and B. Fernández, Glutamine synthetase in brain: Effect of ammonia, *Neurochem. Int.*, 2002, **41**, 123-142.

15. A. K. S. Dhanasiri, J. M. O. Fernandes and V. Kiron, Glutamine synthetase activity and the expression of three glul paralogues in zebrafish during transport, *Comp. Biochem. Physiol.*, 2012, **163**, 274-284.

16. L. A. Sanderson, P. A. Wright, J. W. Robinson, J. S. Ballantyne and N. J. Bernier, Inhibition of glutamine synthetase during ammonia exposure in rainbow trout indicates a high reserve capacity to prevent brain ammonia toxicity, *J. Exp. Biol.*, 2010, **213**, 2343-2353.

17. D. J. Randall and T. K. N. Tsui, Ammonia toxicity in fish, *Mar. Pollut. Bull.*, 2002, **45**, 17-23.

18. P. A. Wright, S. L. Steele, A. Huitema and N. J. Bernier, Induction of four glutamine synthetase genes in brain of rainbow trout in response to elevated environmental ammonia, *J. Exp. Biol.*, 2007, **210**, 2905-2911.

19. Y. Yoshida, T. Chiba, F. Tokunaga, H. Kawasaki, K. Iwai, T. Suzuki, Y. Ito, K. Matsuoka, M. Yoshida, K. Tanaka and T. Tai, E3 ubiquitin ligase that recognizes sugar chains, *Nature*, 2002, **418**, 438-442.

20. L. Bertram, C. M. Lill, and R. E. Tanzi, The genetics of Alzheimer disease: Back to the future, *Neuron.*, 2010, **68**, 270-281.

21. D. Puzzo, L. Privitera, M. Fa', A. Staniszewski, G. Hashimoto, F. Aziz, M. Sakurai, E. M. Ribe, C. M. Troy, M. Mercken, S. S. Jung, A. Palmeri and O. Arancio, Endogenous amyloid-ß is necessary for hippocampal synaptic plasticity and memory, *Ann. Neurol.*, 2011, **69**, 819-830.

22. S. H. Tyan, A. Y. Shih, J. J. Walsh, H. Maruyama, F. Sarsoza, L. Ku, S. Eggert, P. R. Hof, E. H. Koo and D. L. Dickstein, Amyloid precursor protein (APP) regulates synaptic structure and function, *Mol. Cell Neurosci.*, 2012, **51**, 43-52.

23. G. Atkin, E. Minakawa, L. Sharkey, N. Tipper, W. Tennant and H. L. Paulson, *J. Biol. Chem.*, 2014, **289**, 7038-7048.